J Seismol
https://doi.org/10.1007/s10950-025-10308-w

RESEARCH

High-resolution temporal variations in rock elasticity at kiruna mine (block #30 to #34) using full 4D passive seismic tomography

Nicola Piana Agostinetti · Christina Dahner · Savka Dineva

Received: 13 March 2025 / Accepted: 16 June 2025

Abstract We investigate seismic velocity changes in the rock mass related to mining induced seismic events and ore exploitation by computing a one-month long 4D elastic model of Kiirunavaara mine (Sweden). We focus on a specific mine sector, where a single M_W=2.0 event occurred on May 22 (02:31 local time), damaging the infrastructure. We make use of P- and S-first-arrival times obtained from the permanent seismic system for computing the full 4D (continuous 3D volume in time) seismic velocity model of Kiruna mine using a trans-dimensional Monte Carlo sampling. The trans-dimensional approach guarantees that the resolution, both in space and in time, is strictly data-driven. Our results give the following insights into the velocity differences at the mining levels and at different time-length scales. (a) We observe a striking correlation between spatial variations of V_P and ore-body geometry, confirming the robustness of the velocity model. Clay zones appear as a low V_P / V_S ratio zones, as seen in previous tomographic studies. (b) High-frequency (hourly) fluctuations of the rock mass V_P around the ore-passes are highly correlated with seismic sequences in the same rock volumes. In particular, V_P increases rapidly when ore-passes are seismically active and V_P values keep a high value for few (1-4) hours after the end of the seismic sequence. (c) The smoothed velocity model, computed as averaged model over a 2-days moving window, suggests that low-frequency V_P fluctuations can be compared to stress cell measurements located closely.

Keywords Passive seismic tomography · Mining induced seismicity · Bayesian inferences

Supplementary Information The online version contains supplementary material available at https://doi.org/10.1007/s10950-025-10308-w.

N. Piana Agostinetti
Department of Earth and Environmental Sciences, Universitá di Milano-Bicocca, Piazza della Scienza 4, 20126 Milano, Italy

N. Piana Agostinetti (✉)
Department of Geology, University of Vienna, Vienna, Austria
e-mail: nicola.pianaagostinetti@unimib.it

C. Dahner
Luossavaara-Kiirunavaara AB, LKAB, Kiruna, Sweden
e-mail: christina.dahner@lkab.se

S. Dineva
Department of Civil, Environmental and Natural Resources Engineering, Lulea University of Technology, Lulea, Sweden
e-mail: savka.dineva@ltu.se

1 Introduction

Variations in elastic rock properties during production have been widely recognized in seismically active underground mines using passive seismic tomography. Usually they are associated with different phenomena: excavation (Qian et al. 2018), seismic sequences (Ma et al. 2020), blasting, and moderate seismic events with rockbursts (before and after them) (Cai et al. 2015; Young and Maxwell 1992). The co-existence of sev-

Published online: 01 July 2025

eral factors can prevent the correct association of a particular pattern of elasticity variations to a single phenomenon.

We investigate elastic rock properties (in terms of P-wave velocity, V_p, and of the ratio between P-wave and S-wave velocities, V_P/V_S ratio) before and after a damaging seismic event ($M_l = 2.0$) in occurred in Kiruna-Luossavaara Mines (Lapland, Northern Sweden), carefully selecting one sector of the mine and one month time-window (before and after the event) where one single "moderate" (i.e. potentially damaging) seismic event occurred within on-going production activities. We make use of a novel methodology, the *full 4D travel-time tomography*, for computing passive seismic tomography (Piana Agostinetti 2021; Piana Agostinetti and Calo 2014, 2015), an alternative methodology to *time-lapse tomography* (Caló et al. 2011; Chiarabba et al. 2009; Qian et al. 2018). Standard time-lapse tomography is based on the repetition of the standard 3D tomography analysis, using portions of the seismic data recorded in user-defined time-windows. The choice of such time-windows strongly affects the results, potentially masking temporal variations in elasticity characterized by a periodicity not represented by the selected time-windows. On the other hand, the full 4D travel-time tomography enables exploiting seismic data to retrieve continuous variations of rock elasticity in time. The full 4D travel-time tomography does not operate with user-defined time-windows and it computes an elastic model that is continuous in space and time. Removing the subjective partition of the time-axis avoids the risk related to the not proper choice of the length of the time-windows for monitoring unknown phenomena. In other words, the full 4D tomography does not operate on time-windowed data. Standard time-lapse tomography routinely defines sub-sets of the entire data occurred in the investigated period, where each subset encompasses all the data in a predefined time-window. Conversely, full 4D tomography considers all the data in the investigated period at the same time. An approach derived from the full 4D tomography method has been recently applied to volcano seismology (Giacomuzzi et al. 2024, 2025). In general, the full 4D seismic tomography approach is suitable for studies in which the phenomena under investigation, and especially their time-evolution, are largely unknown. The details for developing the full 4D seismic tomography are given in the Supplementary Information (SI) on the Journal website.

The aim of this work is to monitor the changes of stress in the rock mass, in large volumes of mines. The monitoring task is delivered by applying a methodology based on the full 4D travel-time tomography. The real-world case illustrated in this study makes use of seismic data recorded in the Kiirunavaara mine, in a section of the mine approximately 0.6 km long 0.6 m wide and 0.4 km thick. We first present the monitoring workflow together with the description of some critical parameters. Then, we show the results obtained with one month of data, in terms of an average model of mine's seismic velocities, and velocity fluctuations on the short- (6 hours) and long- (2 days) terms. Results are analyzed in terms of: 1) correlation between the average velocity model and known geological features; 2) correlation between the velocity changes and ore-pass activity as well as production blasting; 3) correlation between velocity changes before/after the 'moderate' $M_l = 2.0$ event on May 22, 2016 and the available in-situ stress data in the same area. A critical review of the obtained 4D model is made with conclusion about future use of the new methodology in seismically active mines.

2 Data and methodology

On May 22, 2016 (02:31 local time, 01:31 UTM): (a) a $M_l = 2.0$ seismic event occurred in Kiruna close to the ore-passes in Block 34 causing damage at the infrastructure in production levels at depth 1079 m and 1108 m; (b) no other event with $M_l > 1.0$ has been recorded in the same area, in the previous three weeks; and (c) the seismic system recorded a regular level of seismic activity in the same month, close to the ore-passes in both B30 and B34, generating a sufficient number of seismic data (i.e. P- and S-phases/arrival times) to be used as input for our passive seismic tomography. The hypocentral depth of the $M_l = 2.0$ event has been estimated by different analysts between 1112 m and 1172 m, depending on the seismic data used for the location and the location methodology. Given the distribution of the seismic stations, the uncertainty in the location of the seismic event could be estimated in few tens of meters (see also Piana Agostinetti et al. 2023) for a test about the precision of the location of seismic event in Kiruna. Our study volume (area) encompasses B30 and B34 in Kiirunavaara mine, between X=6000-6700 and Y=2800-3600 We focus our analysis on the depth lev-

els Z=800-1400 m. We select May 2016 as one-month time-window including 21 days before and 8 days after the seismic event on May 22. In such time-period and investigated volume, we found 35,978 events in the LKAB seismic catalogue.

We make use of a passive seismic tomography algorithm for reconstructing the rock mass velocity in time and space within the study area. The monitoring workflow is based on the algorithm described in Piana Agostinetti et al. (2015), re-casted to a mining setting. Briefly, the workflow integrates the algorithm with additional necessary steps: (1) a Monte Carlo event location; (2) the full 4D travel-time tomography (modified from Piana Agostinetti et al. 2015); and (3) the post-proscessing steps for defining the most robust features in the 4D model.

A preliminary Markov chain Monte Carlo (MC) location of each single seismic event is performed, following the approach described in Riva et al. (2024), collecting 1 Million of locations per event. Such locations are used to estimate uncertainties in hypocentral parameters. Events with location uncertainties less than 20 meters, on each component, are selected to be used as input to the tomography.

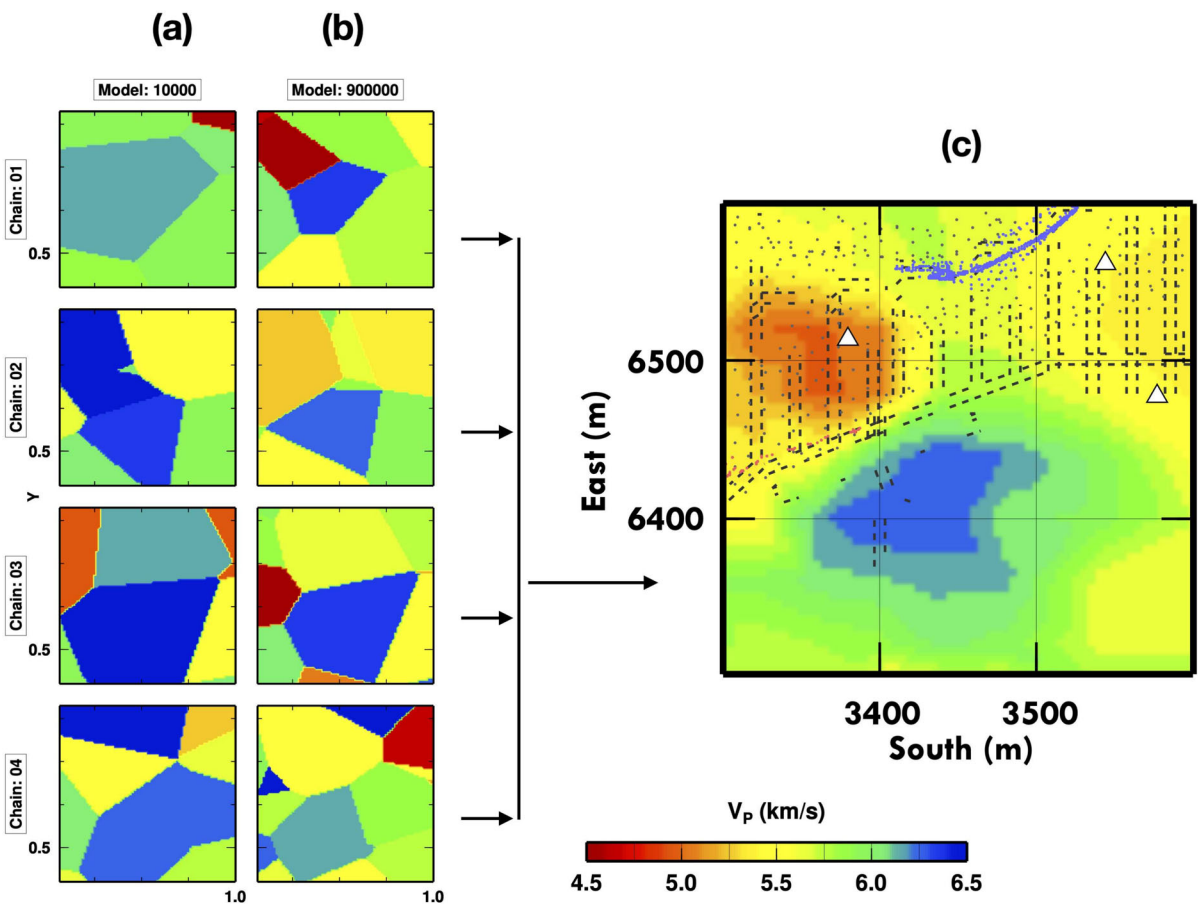

Fig. 1 Example of 4D Voronoi elastic models collected along the trans-D McMC sampling. Here, we show the details as a 2D slice of the 4D model (at depth 1120 m, and time: 12:00 26/05/2016). (a) 2D slice of the 4D Voronoi models for the four independent Markov chains, in the initial stage of the McMC sampling (model # 10 000). The models are still resembling the starting model (randomly extracted from the priors) and they do not show any similarity. (b) 2D slice of the 4D Voronoi models for the four independent Markov chains, in the final stage of the McMC sampling (model # 900 000). Here the four models are much more similar, due to the convergence of the McMC sampling to the PPD, showing a central high velocity patch, with a low velocity patch in the upper left corner. Note that in panels (a) and (b) the coordinate system indicates the normalized values, as detailed in the Methodology section. (c) Mean posterior of the elastic model, presented as 2D slice of the full 4D PPD model

The full 4D travel-time tomography is used to define the variations of the velocity of the rock mass in time. Such algorithm has been previously applied to geothermal research (Piana Agostinetti and Calo 2014, 2015) for identifying elasticity variation during geothermal well stimulation phases. The full 4D travel-time tomography is based on the algorithm presented in Piana Agostinetti et al. (2015) and the detailed workflow is presented in Piana Agostinetti (2021). It comprises a trans-dimensional (trans-D) Markov chain Monte Carlo (McMC) sampling of solutions to the tomographic inverse problem (Malinverno 2002; Sambridge et al. 2006), where velocity is not limited to variations in space, but can assume different values in time. In this way, the method is able to define a full 4D velocity model (parametrized as an ensemble of 4D Voronoi cells), without any time-slicing pre-defined by the user. The trans-D behaviour enables to retain in the model only features fully supported by the data (Fig. 1), i.e. spatial structures and time-variations are data-driven, not imposed by the user (the so called "parimoniosity" Malinverno 2002). The key-modifications of the algorithm, with respect to Piana Agostinetti et al. (2015), are listed in the Supplementary Information (SI).

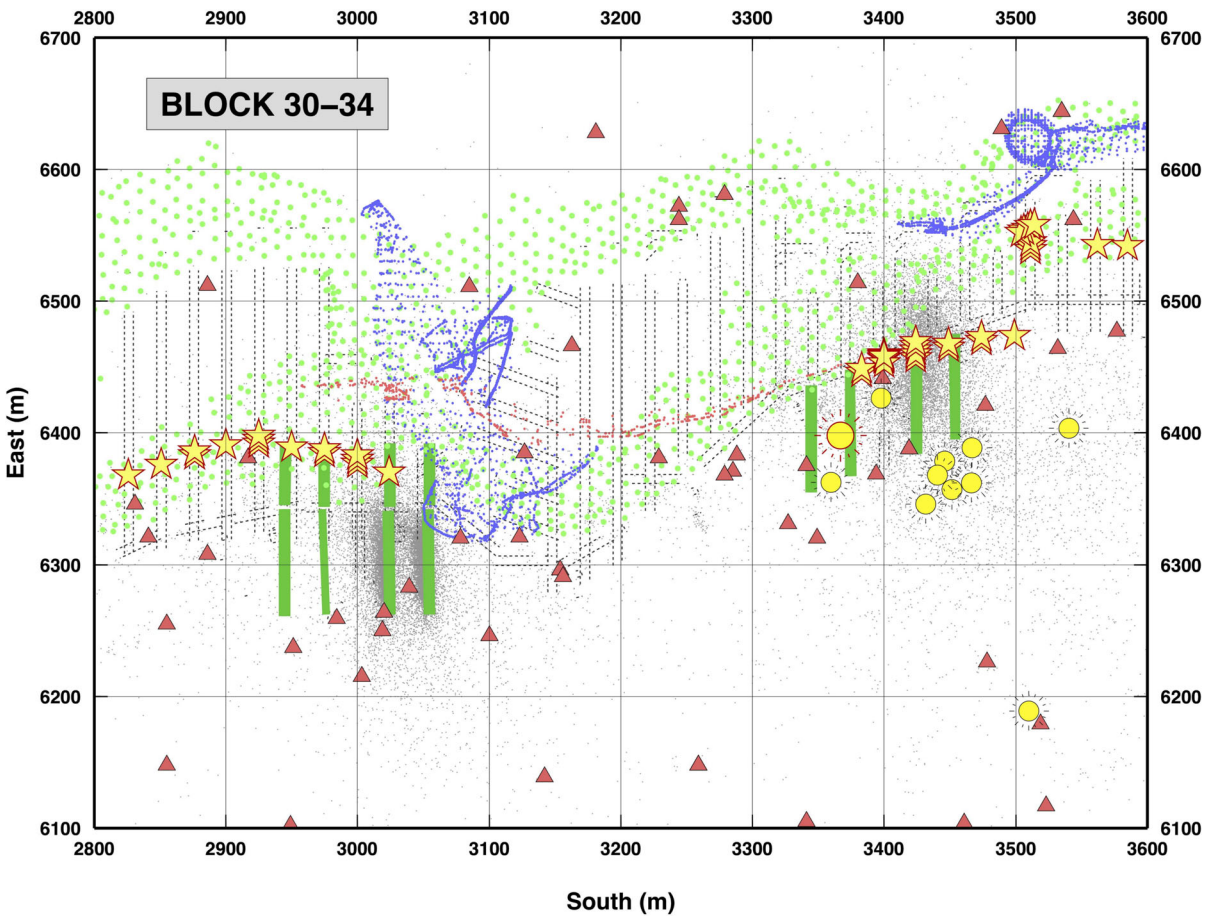

Fig. 2 Map of Blocks 30 and 34 in Kiirunavaara Mine with the input data used in the study. Grey dots indicate preliminary locations of seismic events that occurred in the study area during May 2016. Yellow suns show the position of the relevant seismic events ($M > 1.0$), and a large yellow sun with red contour displays the location of the M=2.0 that occurred on May 22, 2016 which caused damage to the infrastructure (approximate location: X=3350 and Y=6400). Red triangles display seismic sensors. The infrastructure is depicted with dashed lines (1108 m production level is plotted). Ore passes are drafted as green thick lines. Yellow stars indicate locations of production blasts (mainly occurring at 1051 m and 1021 m production levels). Coloured dots show the extension (at level 1120 m) of the geological features: green - ore body; red - dykes; purple - clay zones

Finally, we obtain a collection of 120 Millions of 4D elastic models of the mining area and 1 Million of locations for each single event, which are post-processed to be easily interpreted. Given our sampling strategy, the collection of 4D elastic models and the event locations are distributed according to the posterior probability distribution (PPD) and Bayesian inferences can be used to extract information on the investigated parameters. The relocated seismic catalogue of May 2016 is generated as the mean PPD of the event locations, together with the standard deviation (std) of the PPD, and includes picking quality (i.e. residuals) for evaluating single event location. The mean PPD of the elastic model is extracted from collection of 4D elastic models and is represented as a numerical model of the mine: a 1-hour time-lapse 3D model of V_P and V_P/V_S ratio for the examined volume, with a grid spacing as small as 40x40x40 m (for a total of 721 3D elastic models). For each single 3D model, the std of the PPD is also computed to evaluate the uncertainties on the elasticity at a given time and space. It is worth noticing that, while we compute the PPD of a full 4D elastic model of the mine, the results are presented as 3D marginal PPD models at given times, to better compare the model

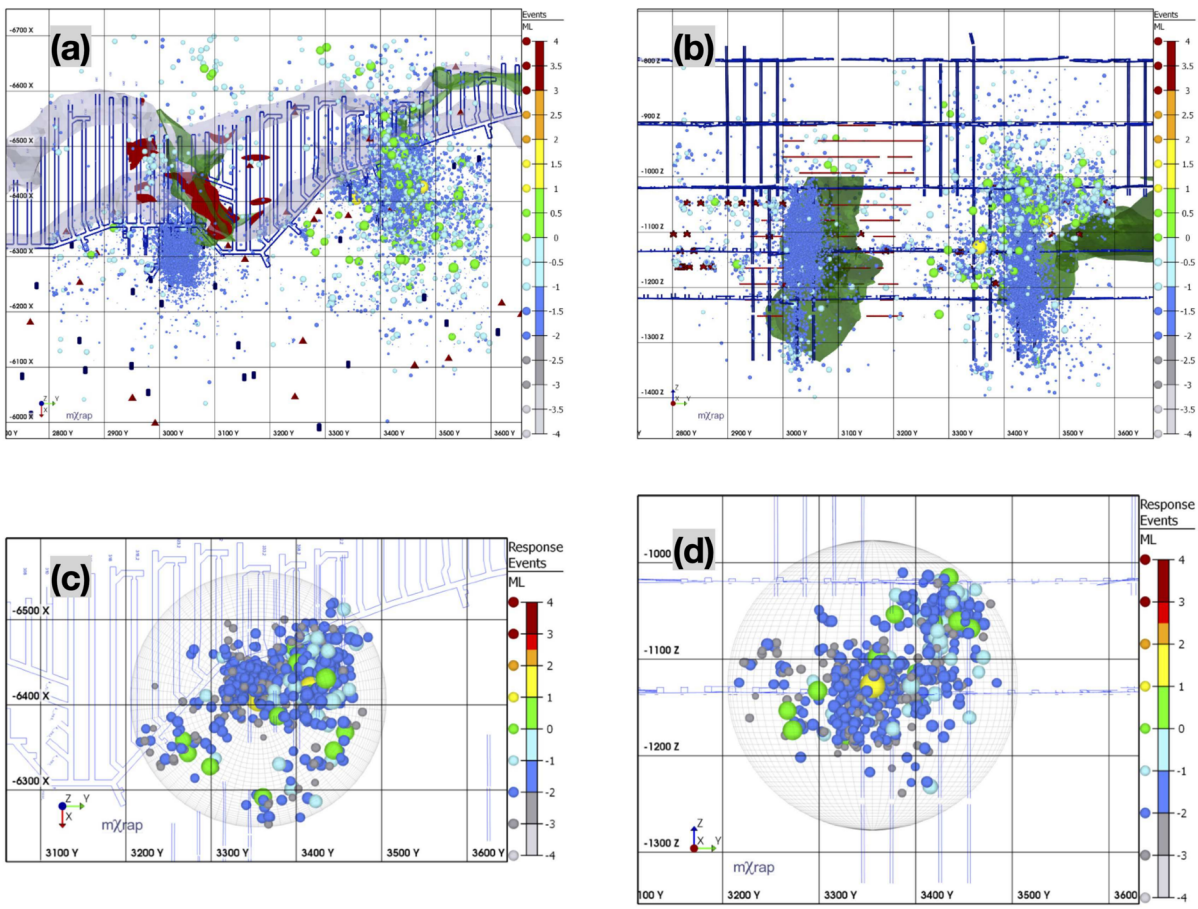

Fig. 3 Map of Blocks 30 and 34 in Kiirunavaara Mine with the input data used in the study. Coloured circles indicate preliminary locations of seismic events that occurred in the study area during May 2016. Colours and dimension of circles refer to magnitude. The large yellow circle displays the location of the M=2.0 that occurred on May 22, 2016 which caused damage to the infrastructure. Blue lines depict the infrastructures. Grey bands indicate the position of the ore. Coloured areas refer to geology: green – clay zones; red – dykes. Red triangles and blue rectangles show seismic network distribution. Red stars report blast position. (a) Map view at 1120 m depth. (b) Longitudinal profile of the mine. The blue vertical lines show the position of the ore-passes. (c) Map view of the area of the M=2.0 event that occurred on May 22, 2016. The events shown are only those associated to the aftershock sequence. (d) Longitudinal profile of the area of the M=2.0 event that occurred on May 22, 2016

with the external information (e.g. geology, blast locations) The final output is compared to seismic event locations, production data, and geological features to interpret the velocity fluctuations. The collection of velocity models is also analysed to define a "static" velocity model, i.e. the average 3D model for the entire time-window and a "low-frequency" velocity model, i.e. a 2-days averaged time-lapse 3D model of V_P and V_P/V_S ratio for the examined volume. In Figs. 2 and 3, we show the input data used in the study, together with external data used for evaluating the results: geological features, infrastructures, production activities and seismicity. In Fig. 4, we qualitatively report waveforms for one seismic event in Kiruna. Both P-wave and S-wave arrivals are clearly visible at a wide range of distances from the source. Data for the analysis (i.e. P-wave and S-wave arrival times) are obtained routinely (manually) from the existing underground seismic system in the Kiirunavaara mine, consisting of almost 100 geophones with corner frequency 4.5 and 14 Hz. Most of the geophones are installed in the footwall of the ore body, with an average minimum interstation distance of about 50m.

2.1 Technical details on elastic model computation

We here report in details, the general model assumptions for both MC relocation process and 4D tomography, to enhance the repeatability of the results and for future comparison with other approaches. MC relocation is obtained independently for each event (single event location) in a uniform half-space. In this way, V_p and V_P/V_S ratio can vary from one event to the other. Obviously, this assumption could seem un-realistic for close-by events in time (one could be tempted to use the same V_p and V_P/V_S ratio for consecutive events). However, estimated V_P and V_P/V_S ratios should be considered as "apparent V_P and V_P/V_S ratio" as they include, for example, the effects of the presence of voids or the heterogeneity of the ore-body. Those apparent V_P and V_P/V_S ratios can in princi-

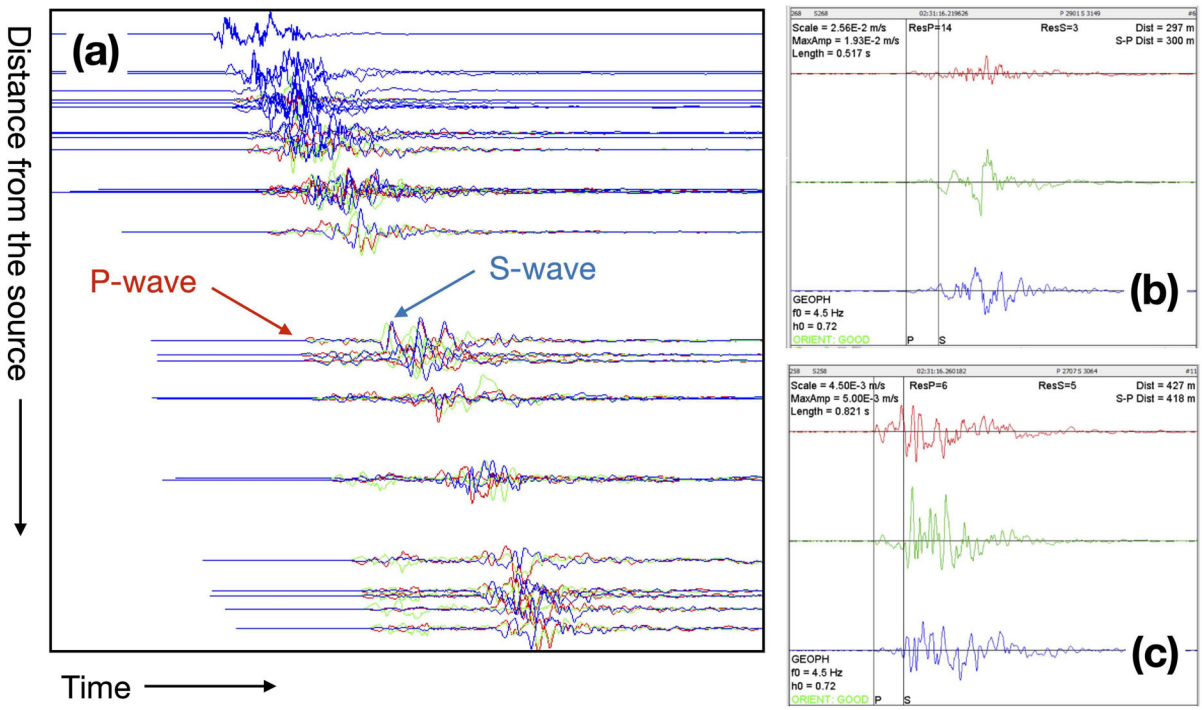

Fig. 4 Example of seismic data recorded in Kiruna Mine. (a) Recordings of the M=2.0 event that occurred on May 22, 2016. Coloured traces reports the three component recordings (if present). (Panels b-c) Details of the 3D recordings for two selected seismic stations: (b) Sensor: 268, distance 297 m; (c) Sensor: 258, distance 427 m

ple show large variations from one event to the next. The algorithm at the base of the full 4D tomography is described in details in Piana Agostinetti et al. (2015) and Piana Agostinetti (2021), with some modifications. Here, we make use of uniform priors for the elasticity and event location, which are more realistic for a highly heterogeneous geological setting as a mine can be. We use a 20x18x16 grid (5760 nodes) for ray-tracing, with 40m spacing in the center of the examined area, between Y= 3000 - 3480, X= 6120 - 6560 and Z= -920 - -1320. This is the so called "computational grid" and defines the maximum spatial resolution in our elastic model.

2.1.1 Priors

MC algorithm for event relocation makes use of uniform priors for both event position and velocity. Prior boundaries for event position are set as large as almost the entire Kiruna mine (Y between 0 and 4700 m, X between 5000 and 6700 m, and Z between -1600 and -200 m). For P-wave velocity (V_P), we consider a broad range of values, given the heterogeneities of the geological units, between 4000 m/s and 8000 m/s. The ratio between P-wave and S-wave elocities (V_P/V_S ratio) ranges between 1.5 and 1.9. In the case of the 4D tomography, we use the following uniform prior probability distributions: on the number of elastic nuclei, between 0 and 2000; on V_P, between 3500 m/s and 7500 m/s; on V_P/V_S ratio, between 1.6 and 2.0; for event position, between -40 and 40 m around the mean posterior position found in MC relocation. Logoritmic value of the scaling factor of data uncertainties can vary between -1 and 3, indicating an error between 1/10 and 1 000 times the sampling rate. I.e. $\sigma(\mathbf{m}) = 10^{\pi_P}\sigma_0$, with $\sigma_0 = 1/6000$.

2.1.2 Overlapping scheme for tomography execution on cluster

To increase the efficiency of the computation and to have a less failure-prone approach, we divided the entire pool of data in 2-days data-batches and adopted a 50% overlapping scheme. In this way, we have 30 data-batches, each 2-days long. Each single data is included in two consecutive data-batches. The gain on efficiency is counter-intuitive, as each single datum is modelled twice. However, having smaller data-batches makes the McMC sampling shorter (1 Million models per McMC sampling). Moreover, the overlapping scheme adopted can easily handle failures in the computer cluster, as a single failure would destroy a single McMC sampling and, thus, would involve a single data-batch (2-days of data) leaving the other data-batches unaffected. In the final 1-hour time-lapse 3D model, each single data-batch fully contributes to the model between 4 am of the first day and 8 pm of the second day (i.e. it has a weight of 0.5, giving the fact that each hour is computed in two consecutive batches). The very first and very last 4 hours have a decreasing importance in the model, going to 0.1 at midnight.

2.1.3 Execution time

The full computation of the 4D elastic model has been executed on a research cluster using between 64 and 256 CPUs per independent McMC sampling. Different data-batches lasted between 12 and 65 hours of computation per chain, depending on the number of events included in the 2-days data-batches. The selected overlapping scheme implies that each recorded phase is modelled twice (thus, we almost double the CPU time requested). Considering that: (a) we selected about 19 000 high-quality events with about 336 000 phases, each event belonging to two data-batches; (b) we divided the data in 30 overlapping data-batches; (c) we ran 4 independent chains per data-batch; and (d) each chain was 1 Million models long; we computed 2 x 336 000 x 30 x 4 x 1 000 000 $\sim$ 80 x 10^{12} forward solutions. Total CPU execution time is about 361 000 CPU-hours (about 1.3 x 10^9 s). We note that McMC sampling can be slow in convergence to the target distribution, here the PPD, thus we collected long chains of models for each data batch, discarding the initial phases. In details, for each chain, we discarded the first 200 000 models as the so-called "burn-in" period, where the sampler is likely not to correctly sample the PPD. After that, one model every 100 is retained for the computation of the PPD.

2.1.4 Bhattacharrya coefficients

Bhattacharyya coefficients (BC) can be used to measure the distance between two probability distributions (Bhattacharyya 1943). A Bhattacharyya coefficient close to 0 means that two probability distributions are almost overlapping, i.e. they are indicating a similar probability distribution. Here, we use BC as a

proxy for measuring the robustness of time-changes in seismic velocities. In case of Gaussian distributions, as our mean and std PPD used to compose the 1-hour time-lapse 3D model, we can use the formula:

$$BC(\alpha_1, \alpha_2) = \frac{1}{4}\log\left(\frac{1}{4}\left(\frac{\sigma_1^2}{\sigma_2^2} + \frac{\sigma_2^2}{\sigma_1^2} + 2\right)\right) + \frac{1}{4}\left(\frac{(\alpha_1 - \alpha_2)^2}{\sigma_1^2 + \sigma_2^2}\right) \quad (1)$$

where α_1 is the mean posterior value of the parameter at time t_1 , α_2 is the mean posterior value of the parameter at time t_2, σ_1 is the posterior standard deviation of at time t_1, and σ_2 is the posterior standard deviation at time t_2 (Ray 1989). In our case, α can represent V_P or V_P/V_S ratio. The 1-hour time-lapse 3D model of the Bhattacharyya coefficient compares the present elastic model (i.e. the 1-hour time-lapse 3D model of the elasticity at a given hour) to the "static" 3D elastic model, i.e. the averaged elastic model over the entire month, considering a minimum standard deviation σ for V_P equals to 10 m/s, and for V_P/V_S ratio equals to 0.01 (see Section 3.2). Obviously, the 1-hour time-lapse 3D model of the elasticity can be used to compute Bhattacharyya coefficients between any pair of hours in the model (e.g. for two 3D models with a 6 hours lag-time), using the same formula, for the analysis of short-term variation of the elasticity.

3 Results

3.1 Re-located seismicity using monte carlo approach

We relocate all seismic events using a Monte Carlo algorithm, where we adopt a Hierarchical Bayes approach . Such approach allows to evaluate the picking errors (i.e. the residuals), so that picking quality is not dictated by the user, but re-defined by the data (and hypothesis) themselves. Overall, picking errors for P-phases are close to $5 \times \sigma_0$ s, where σ_0 is the sampling interval (here 1/6000 s), while picking errors for S-phases are close to $6 \times \sigma_0$ s. It is worth to remember that such estimated picking errors include errors given by the simplified forward modeling considered here (straight-rays in a homogeneous half-space) and thus should not be considered as formal picking errors. Location errors are within 30 m on average, on all components ($X \leq 23$ m, $Y \leq 28$ m, $Z \leq 29$ m), with Y and Z having similar values due to the similar sensor distribution in such directions.

Using our location uncertainties, we select data for the next steps of the analysis (i. e. the 4D tomography). From the original pool of 35,978 events, we select 19,936 events with location uncertainties less than 20 m to be used as input in the tomography workflow. We also observe that picking error (i.e. residual) is a less robust indicator for the quality of the event location. We suggest to avoid using residuals as a parameter for selecting events for the tomography. Finally, we observe that "highly precise" events (location error less than 5 m) can be used to study very specific rock volumes. In Fig. 5, we show the highly precise event locations close to B30 ore-passes. Local seismic clusters can be easily associated with different segments of the ore-passes for further investigations (e.g. computing local b-value, investigation of rock mechanical processes etc.)

3.2 Average velocity in the rock mass in the study area for may 2016

To better assess the robustness of our investigation, we compute an average "static" 3D velocity model for the entire month, i.e. we compute a single 3D model as the average of all velocity models, which represent our 4D information on the study area. It is worth noticing that such model is not only representative of the velocity of the original rock mass, but can still contain information about different phenomena that occurred in the examined volume, if such phenomena occur regularly (e.g. blasting, ore pass activity).

In Fig. 6, we show the "static" 3D velocity model as a map-view of V_P and V_P/V_S ratio at level 1120 m. We observe a general agreement between the spatial distribution of V_P and the ore geometry (here seen as the $V_P = 5.8$ km/s contour), suggesting the robustness of the tomography workflow. The clay-zone close to B30 ore-passes seems to have a low V_P value (Fig. 6b). The clay zone is more pronounced by low values on the V_P/V_S ratio model (Fig. 6c). Such low V_P/V_S ratio values have been previously seen by Berglund et al. (2021), using a different workflow for passive seismic tomography. We can point out that the high V_P anomaly at the B30 ore-passes does not correlate with any mapped geological feature. Most probably it appears in the "static" 3D model due to the sustained seismicity close to the ore-pass during the entire month.

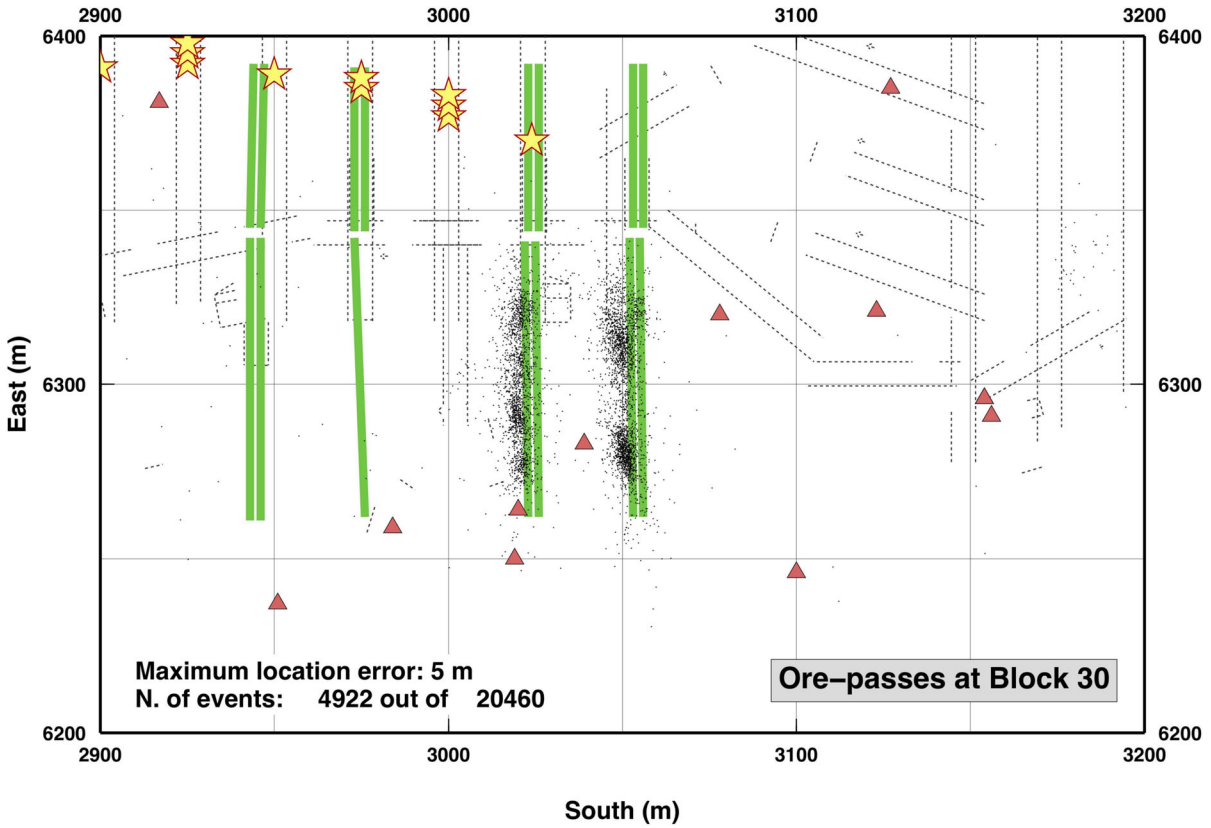

Fig. 5 Precisely relocated seismic events close to B30 ore-passes. Black dots represent the relocated events (4,922 out of 20,460 occurring in the same area) for which an error lower than 5 m has been obtained for each coordinate. Red triangles display seismic stations. The infrastructure at level 1108 m is depicted with dashed lines. Ore passes are drafted as green thick lines. Yellow stars indicate production blast that occurred in the area of B30 during May 2016

Similar effect but not so pronounced is observed around the ore passes in B34 (see Section 3.3.3).

3.3 Time-dependent elasticity of the rock mass in the study area for may 2016

3.3.1 How the full 4D tomography works

Before introducing the results obtained for the entire month, we focus on one data batch for one day (2020/05/10) to illustrate how the full 4D model is able to reproduce the observed travel-times. We compare the results obtained from three different inversion schemes based on three different choices for the elastic parameters of the model (i.e. the events considered are the same, and their parameters are treated in the same way in the three inversions). In a first test we make use of an half-space of unknown velocity. Thus, the algorithm adjust the half-space velocity and the event parameters to fit the data and reduce the residuals. A second test is performed using a 3D model (i.e. no time variations) and in the final test we perform our standard full 4D tomography. Clearly, the three different tests are obtained using the algorithm for the full 4D tomography limited, in the first case, the use of only a single 3D Voronoi cell, and in the second case limited to use a variable number of 3D Voronoi cells. This means that events parameters are treated equally in all three tests.

A detail of the results obtained for the three tests is shown in Fig. 7, where the velocity models close to B34 ore-passes are plotted at different hours, together

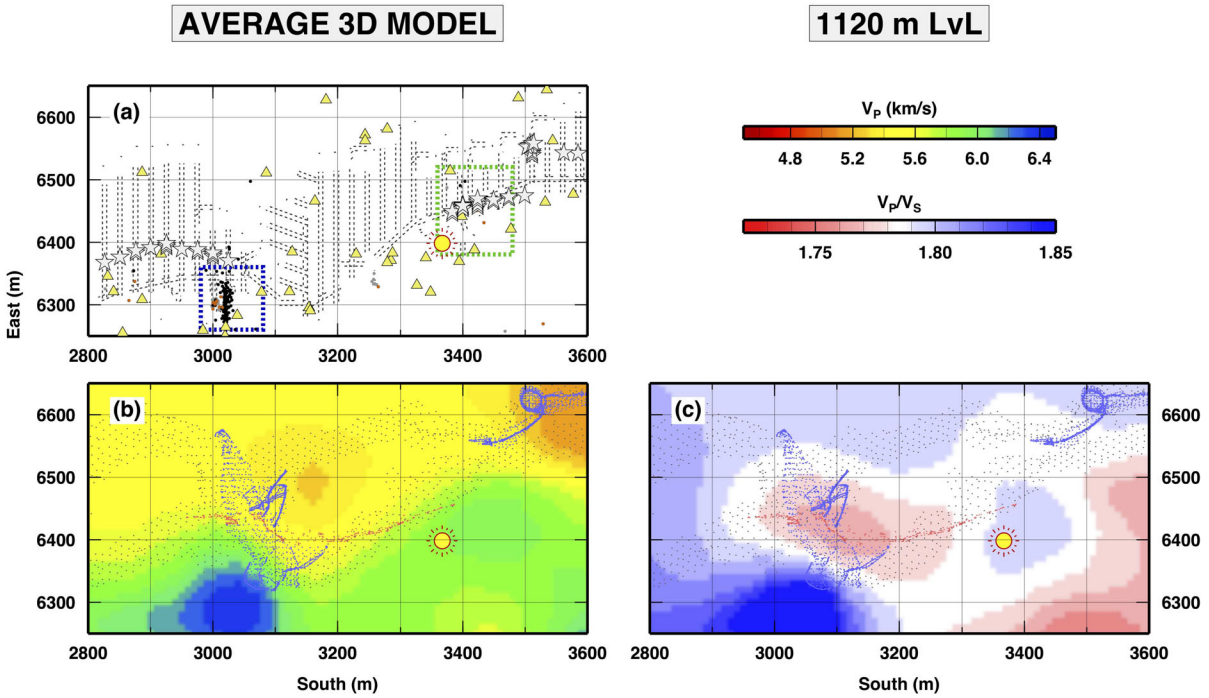

Fig. 6 "Static" V_P and V_P / V_S ratio models as a map of the study area for May 2016, level 1120 m. (a) Seismicity, production blasts and infrastructure. Grey stars indicate production blast location (mainly occurring at production levels 1051 m and 1021 m). Dashed lines depict infrastructures at 1108 m production level. Seismic stations are plotted as yellow triangles. The blue (green) box shows the area around ore-passes at B30 (B34), defined for selecting events used to compute blue (green) histogram in panel (f) in Fig. 8. The hypocenter location of the M 2.0 event is shown for reference (yellow sun). (b) V_P model. Colours represent V_P values, coloured dots show the extension (at 1120 m level) of the geological features: green - ore body; red - dykes; purple - clay zones. The hypocenter location of the Mw=2.0 event is shown for reference (yellow sun). (c) V_P / V_S ratio model. Same symbols as in the panel (b) for V_P model

with the seismicity that occurred in the same hours and the relevant residuals on the observed travel times at the end of the computation. Residuals are represented as the difference between observed travel times and the mean PPD of the synthetic travel times. It is worth noticing that we computed a full velocity model for the entire mine in all the three tests, using all events that occurred on that day (2016/05/10), but we show here in Fig. 7 only the rock volume around the ore-passes at B34, for clarity.

As the velocity model increases in complexity, from top row (the uniform half-space solution) to the bottom row (full 4D model), the residuals are better reproduced, both in terms of a reduced Gaussian width and a reduced shift. In particular, we can observe that the residuals for the uniform test-case are larger than the other test-cases, with S- waves residuals larger than P-wave residuals. In the second case (3D model) we observe a relevant shift in the residuals (positive shift for both P-wave and S- wave residuals). Such shift obtained for the 3D model in principle could be (and generally is) removed using a user-defined starting model (e.g. Kissling et al. 1994). However, such starting model should be expressly defined for each data batch in our workflow, and we would go back to the issue of having pre-defined time-window in time-lapse tomography (exactly the reason why we adopt our full 4D tomography scheme). Finally we observe, from the plot at the bottom of Fig. 7, that the level of the residuals adopting the three inversion schemes is not clearly different (e.g. there is not a scheme that, using an inappropriate phrasing, "reduce the misfit far more than

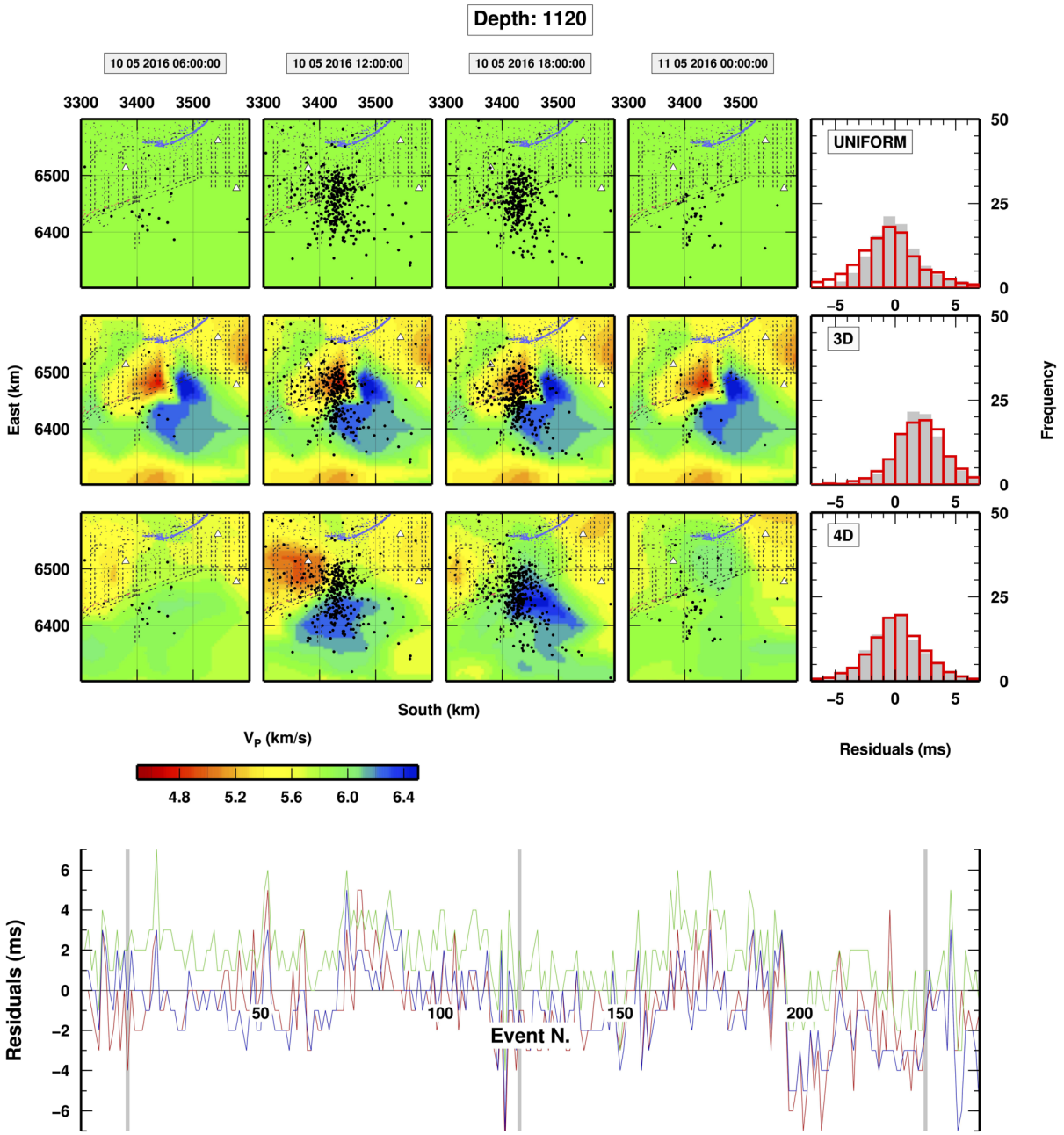

Fig. 7 Comparison of the results for one day, May 10th 2016, obtained using three different inversion schemes: an elastic half-space, a 3D model, and the full 4D model (on the rows from top to bottom). Coloured maps indicate mean PPD V_P models at 1120 m depth level for the area of Block 34 ore-passes, at four different hours: 6:00, 12:00, 18:00 and 24:00 on May 10th 2016. Black dots display seismicity occurring in the indicated time-frame (i.e. three hours before and three hours after the indicated time of the day). Seismic stations (white triangles), geology (purple dots) and infrastructures (dashed black lines) are also shown for references. Histograms on the right represent the residuals, which are computed as the difference between the observed travel-times and the mean PPD of the synthetic travel-times (grey shaded- P waves; red contour- S-waves). On the bottom of the figure, the residuals are plotted as a function of the event progressive number: red line for uniform model; green line for 3D model and blue line for 4D model. Vertical grey lines separate events in the four different time-frames shown in the upper panels, three hours before and three hours after the indicated date-time on top)

the others"), but we need to consider that events can be freely relocated and they adjusted differently in the three schemes to reduce the misfit.

3.3.2 Full 4D elastic model and Bhattacharyya coefficients

The final collection of 120 Million velocity models represent our 4D information on the study area. To represent and interpret such information in conjunction with other sources of information, we computed the 1-hour time-lapse 3D model of V_P and V_P/V_S ratio for the examined volume. For each point on a 40m spaced 3D grid of the mine (4 032 points) and for each hour in May 2016 (721 hours), we measured the mean posterior and the standard deviation of V_P anV_P/V_S ratio across all 120 Million elastic models (the so-called marginal posterior of V_P and V_P/V_S ratio for a given 4D point). Basically, we estimate a Gaussian posterior probability distribution (PPD) for all 4 032x721 points. Such numerical model does not contain all the information collected in the trans-D McMC sampling. For example, it lacks all correlations between velocity at different times, and correlation between velocity and event locations. However, it can be used to visually represent the output of our workflow and to make general interpretations. In particular, as shown in Fig. 8, the PPD can be used to highlight volumes (in time and space) of the mine where the information contained in the input data are not enough to substantially modify the prior information (i.e. where prior and posterior information are close to each other). This is a fundamental asset of the Bayesian approach to seismic tomography because it discriminates where velocity in time and space is defined by data, and where data do not add any significant information.

To evaluate the fluctuation in velocity, we computed the Bhattacharyya coefficients of the 1-hour time-lapse 3D model with respect to the "static" model. Briefly, for each 4D point we computed the BC between the Gaussian PPD to the "static" model, adopting a standard deviation of 100m/s for V_P and 0.01 for V_P/V_S ratio for the "static" model. As a rule of thumb, a BC lower than 0.5 means no difference between two probability distributions, while a BC larger than 1.0 means that the two probability distribution are significantly different. In Fig. 8, we report one frame of V_P and V_P/V_S ratio models, i.e. one hour of the 3D time-lapse models, with associated BC models.

3.3.3 Fast elastic fluctuation related to ore-passes seismic activity

Looking to the 1-hour time-lapse 3D V_P model and the relocated catalogue together, the first feature that becomes immediately evident is the correlation between ore-pass seismicity and V_P changes in the surrounding rock volume. In particular for B30 ore-passes, the "activation" of the ore-passes, i.e. when more than a hundred of seismic events occur in the same hour, coexists with a sharp increase in V_P value for the rock volume containing the ore-passes themselves. Such fluctuations of the V_P model are generally associated to BC>1.0 which indicates their robustness. A preliminary interpretation of the correlation could be attributed to the state of the ore-passes (empty or filled). In case of filled ore-passes, seismic waves can more easily travel through the rock volume, generating an apparent high V_P value for such rock volume. However, more information on the use of the ore-passes at the time of the high-velocity anomalies is needed to interpret our findings. In Fig. 9, we present one example of the fluctuation of the V_P model close to B34 ore-passes. The high V_P anomaly close to the ore-passes appears with the seismic "activation" of the ore-passes and it lasts no more than 6 hours.

3.3.4 Velocity fluctuation during blasting activity

Given the presence of large fluctuations in V_P model associated with seismic activation of the ore-passes and the larger uncertainties in the time-lapse 3D model at production (blasting) levels (1021 m and 1051 m) with respect to level 1120 m, the post-blasting effects on the velocity of the rock mass (if existent) seem to be masked. It is not easy to correlate production data and our time-lapse 3D model. Focusing on level 1120 m model (about 80 m from the blasting location) and analysing the velocity model in the period of low-seismic activity at B34 ore passes (i.e. between May 7 and May 17, 2016, see Fig. 8h), we observe that production blasts occurring between X=3400-3500 and Y=6450-6500 are generally associated with a robust (BC>1) V_P/V_S increase in a limited (max 150m

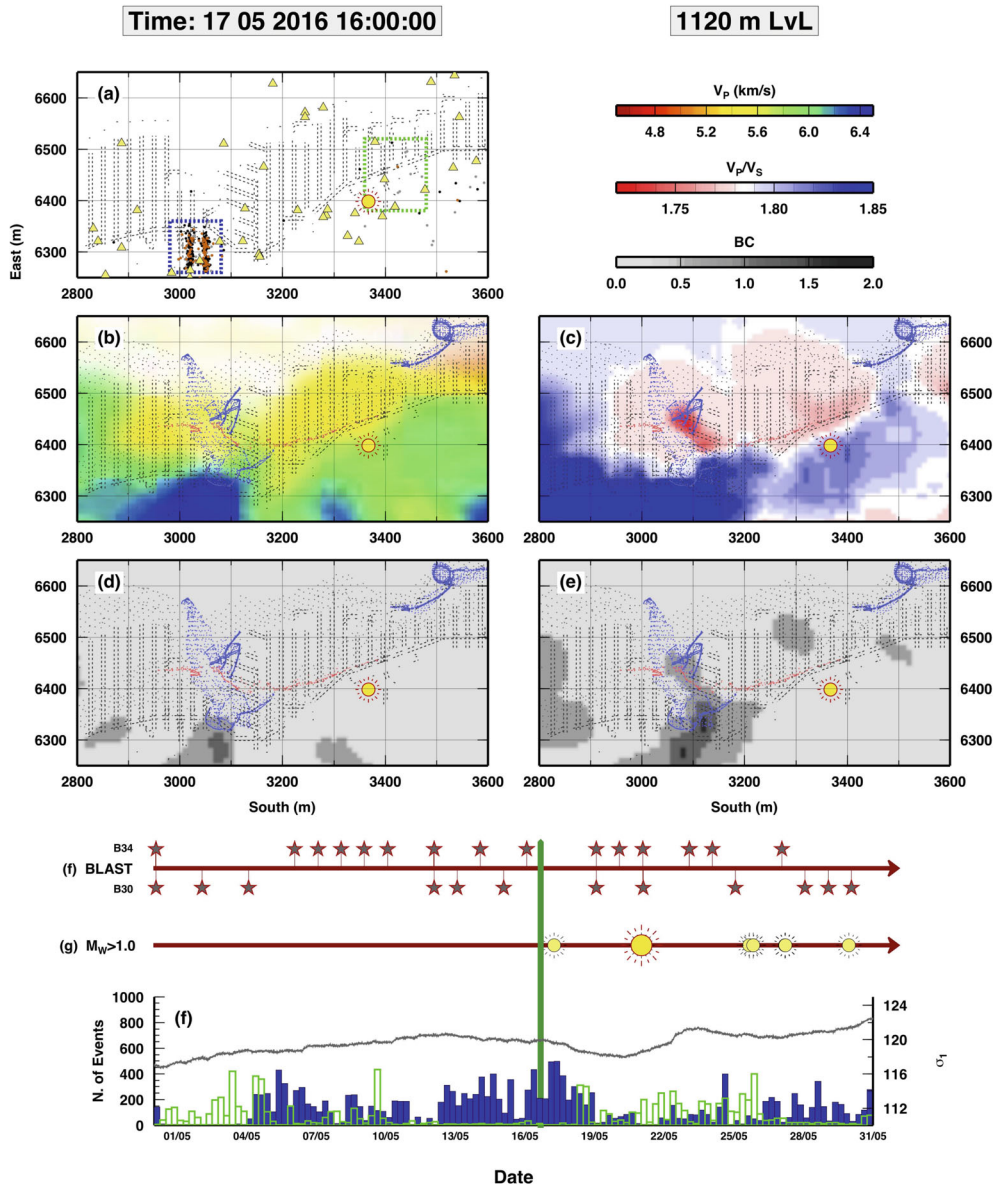

Fig. 8 One *frame* of the full 4D elastic model, for the time: May 17th 16:00, represented as map-views of V_P and V_P/V_S ratio at level 112 0m. For panel (a) to (c), same symbols as in Fig. 6, except for panel (a) where coloured dots represent seismic events: grey- occurred in the previous two hours; red- occurred in the indicated hour; black- occurring in the next two hours. In panels (b) and (c), the whitish colorured areas indicate where the ratio between posterior and prior std is larger than 0.85. (d)-(e) Bhattacharyya coefficients for the V_P and V_P/V_S ratio models in panels (b) and (c), computed with respect to the "static" V_P and V_P/V_S ratio models in Figs. 6b and 6c. (f)-(g)-(h) Time-occurrence of main seismic events and production activities in the study area. Grey stars indicate the occurrence of production blasts, separated for the two blocks. The yellow suns indicate the occurrence Mw>1.0 seismic events. The biggest yellow sun is the Mw=2.0 event. (h) Histograms of the number of seismic events occurring close to ore-passes: green – B34; blue – B30. The grey line indicates the local measurement of maximum stress (σ_1) during May 2016. Additionally a green vertical bar indicates the exact time-step in the time-series for which the elastic model is displayed in panels (b)-(c)

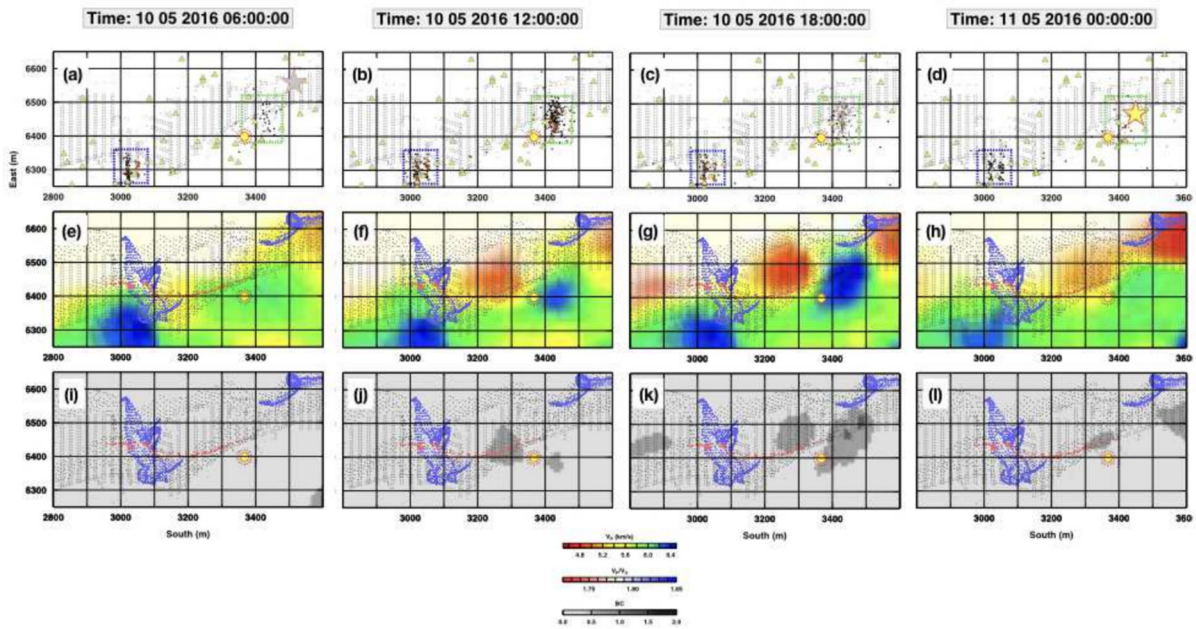

Fig. 9 Example of velocity variations at depth level 1120 m during a seismic sequence close to one ore-pass activation. Each column report the state of the velocity of the mine at different time, starting from May 10th 2016 06:00, every six hours. Panels (a) to (d) show the occurrence of a seismic sequence at B34 ore-passes (i.e. within the green box). Panels (e) to (h) show the map of V_P model in the same time-steps. Panels (i) to (l) show the BC coefficients for the V_P model. Symbols in panels (a) to (d) are the same as in Fig. 8a. Symbols in panels (e) to (h) are the same as in Fig. 8b. Symbols in panels (i) to (l) are the same as in Fig. 8d

radius) area. The transient perturbation in V_P/V_S ratio seems to last between 2 and 4 hours. However, this effect occurs in 4/6 of the cases under observations, with 1 case with unclear rock response and 1 case with opposite (V_P/V_S ratio decrease) effect. We can interpret V_P/V_S ratio increase after blasting as a transient modification (i.e change in fracture aspect ratio) of the local fracture network. The six cases of analysed production blasts at level 1022 m for B34 area are shown in Figs. 10 and 11. Further investigations are necessary on the correlation between the V_P/V_S changes after blasting and post-blast seismicity (spatial correlation between number of seismic events and range of V_P/V_S change). The rough review of both types of data shows some evidences but more cases (blasts) are needed to have a proper quatification for the correlation.

Further investigation is necessary on the correlation between the V_P/V_S changes after blasting and post-blast seismicity (spatial correlation, number of seismic events and range of V_P/V_S change etc). The rough review of both types of data shows some correlation but more cases (blasts) are needed to have a proper expression for the correlation.

3.3.5 Slow variations of the velocity before the M=2.0 event

Stress-cell for monitoring of in-situ stress changes has been installed in B34 (level 1165 m) in 2013 (Dahner and Dineva 2020). Recent investigations on stress-cell data suggested a peculiar precursory pattern for relatively moderate events: a significant drop in maximum stress σ_1 value followed by a $\sim$3 days recovery of the stress level, during which the moderate relevant event occurs (Dahner and Dineva 20200. The pattern has been observed for the M=2.0 event that occurred on May 22, 2016 as well, at a distance of approximately 80 meters from the stress cell. To compare our velocity model variations with stress-cell data recorded in the examined volume, we compute a 2-days time-lapse 3D model that partially removes high-frequency fluctuations associated with ore-pass seismicity. In Fig. 12,

Approximate blasting time in B34 (local time)	Depth lvl	Explosive (kg)	Effect
07/05/16 01:26	1022	8841	Vp/Vs ratio ↓
09/05/16 01:37	1022	9866	Vp/Vs ratio ↑
11/05/16 01:31	1022	5124	Vp/Vs ratio ↑
13/05/16 01:33	1022	*	No effect
15/05/16 01:33	1022	6824	Vp/Vs ratio ↑
17/05/16 01:38	1022	9566	Vp/Vs ratio ↑

* Multi-explosion: 5 charges in close locations, for a total of > 10000 kg

Fig. 10 Table of analysed blasts in Block 34

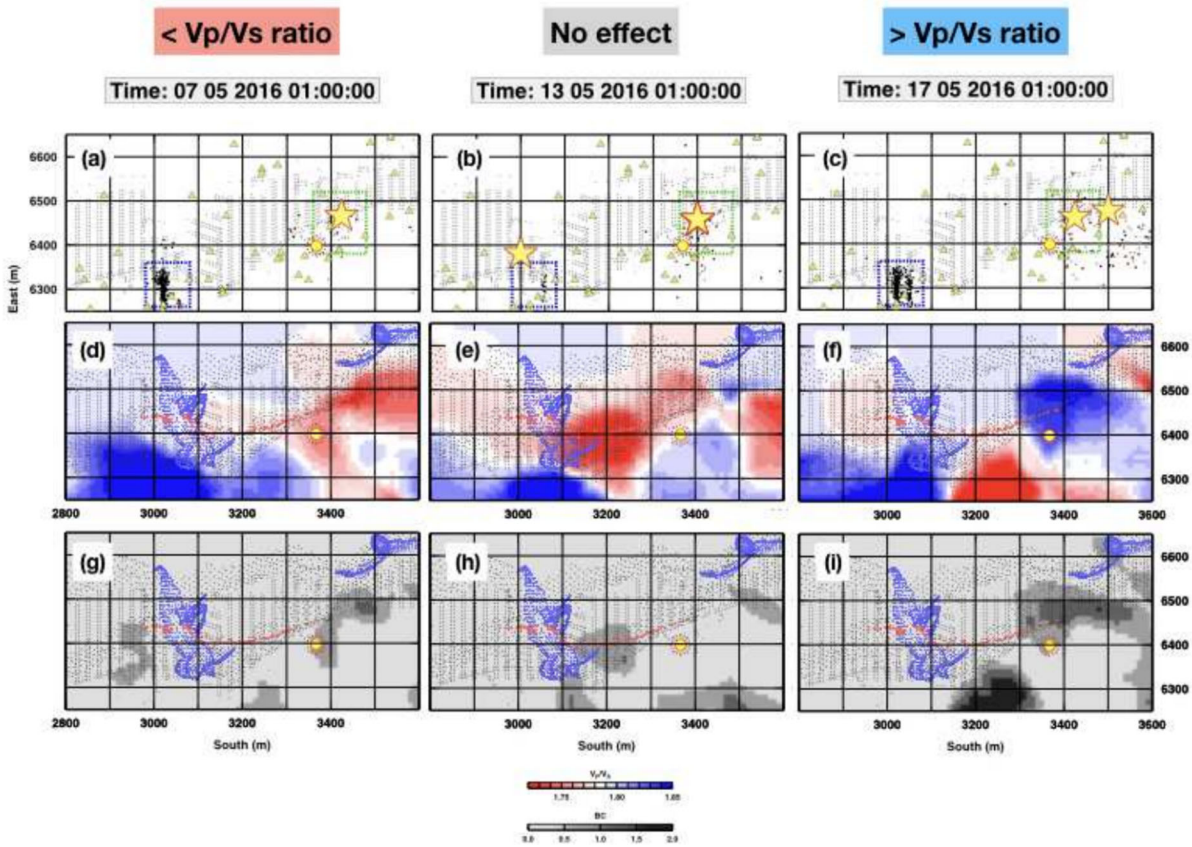

Fig. 11 Examples of variations of V_P / V_S ratio model at depth level 1120 m during production blasts close to B34 ore-passes. Each column reports a different case with: V_P / V_S ratio decreased in the blasting area (left column), no relevant effects (mid column) and (V_P / V_S ratio increased (right column). Panels (a) to (c) show the occurrence of a production blasts at B34 ore-passes (i.e. within the green box). Panels (d) to (f) show the map of V_P / V_S ratio model in the same time-steps. Panels (g) to (i) show the BC coefficients for the V_P model. Symbols in panels (a) to (c) are the same as in Fig. 8a. Symbols in panels (d)- (f) are the same as in Fig. 8c. Symbols in panels (g) - (i) are the same as in Fig. 8e

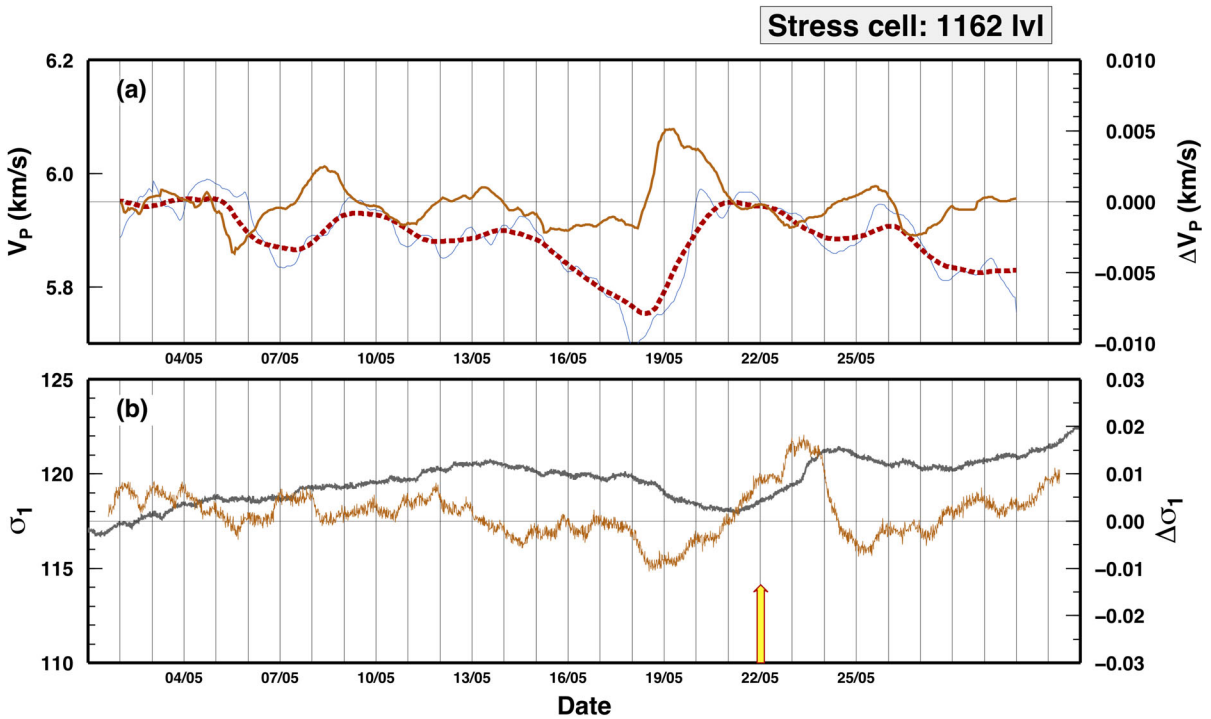

Fig. 12 (a) V_P values as a function of time for the closest grid nodes to the stress cell position (grid node at X=3280, Y=6360; and Z=-1160; stress-cell at X=3281, Y=6377, Z= -1163, distance about 17 m). Blue line are the values from the 2-days smoothed elastic model. Red dashed line is a moving average of the blue line, with 48 hour long window. The orange line represent the derivative of the V_P, computed as the numerical increment at one-hour lag. (b) Local maximum stress (σ_1) from stress-cell data (grey line) and its derivative (orange line). The yellow arrow indicates the time-occurrence of the M 2.0 event

we report both the V_P time-series from the 2-days time-lapse 3D model (panel a) and the stress-cell time-series (panel b). The V_P time-series represents the V_P value of the closest node, on the 40m grid, to the stress-cell. The V_P time-series displays a relevant drop starting one week before the M 2.0 event on May 15, 2016, followed by a rapid increases lasting 2 days (from May 19 to May 21). The M=2.0 event occurs one day after the final recovery of the average velocity (V_P 6.0km/s). The most relevant observation is the correlation between the derivative of V_P value and the derivative of σ_1 value. In fact, the sharp recovery in V_P value and the sudden drop in σ_1 value occur at the same time (positive and negative peaks in early May 19, 2016 for V_P and σ_1, respectively), suggesting that the (sudden) stress drop enables fracture closure (fast increasing V_P), which in turn could facilitate fluid migration and fault lubrication.

4 Discussion

The workflow for monitoring the velocity changes in the rock mass presented in this study is able to reconstruct the mining volume in details following a strict Bayesian framework. In this way, we are able to measure uncertainties on the investigated parameters and to use such estimated uncertainties for both evaluating the time-lapse 3D elastic models in space and time (through the ratio of the std, posterior vs prior) and their variations computing the BC for a given choice of two elastic models. We recognize that such results can be achieved in a seismically active mine as Kiirunavaara, where the number of seismic events per day in the mine sector under investigation never dropped below 1 000. Such huge amount of data could be necessary to define the velocity model with the details presented here. Moreover, we also identify, at the same time, a

potential pitfall in the interpretation of the retrieved time-lapse 3D elastic model. The presence of multiple sources of perturbation of the velocity of the rock mass (here, for example, the co-existence of blasts and ore-passes activation) could make the interpretation of the final results challenging without having additional information from the mine production activities. Thus, considering the monitoring workflow from a strict computational point of view, we can state that such kind of monitoring is definitely available, though its use in active mines should be carefully planned and evaluated.

The full 4D tomography performs a strictly data-driven velocity model evaluation, thus suppressing features not (or partially) supported by data. Comparing to a more standard approach as 3D model (of even the half-space approximation) we can observe that the level of residuals (i.e. generally, and not appropriately here, called the misfit reduction) is limited. This fact points out that information contained in the seismic rays and relative to temporal variations of the velocity of the rock mass is definitely vague. In the geophysical inverse problem solved here, prior and posterior probability distributions are likely to be very similar for many space/time volumes of the mine. Having similar prior and posterior probability distributions indicates that the use of (artificially engineered) proposal distributions in the generalized Metropolis' rule (Gallagher et al. 2009) to boost the McMC sampling it totally useless. In fact in this case, the highest acceptance values are already obtained when proposal distribution is exactly prior distribution.

Positive velocity variations at the ore-passes, i.e. local increases in V_P, are the most striking effect retrieved from our analysis. Such variations could be, in principle, related to stress-increase, if we consider that local stress-increases are related to local increases of seismicity rate (i.e. when stress increases we have more seismic events). However, we should consider that V_P measures in mines are strongly affected by voids and heterogeneities. In this case, we should consider the possibility that empty and filled ore-passes could be "seen" by the seismic rays as different objects. A strict comparison of activities in the ore-passes such as filling level variations are necessary to correctly interpret such velocity variations.

Slow-variations of the seismic velocity of the rock mass close to the stress cell seem to correlate to the characteristic pattern in stress fluctuation found for Kiirunavaara mine before the occurrence of a "moderate", from a mine point of view, events (Dahner and Dineva 2020). The relevantly slow decay in V_P could be related to opening of new fractures or changes of aspect ratio in existent fractures. In this picture, the sudden increase in V_P occurring at the same time of the stress-drop could be given by the closure of the fractures no more sustained by the local stress field.

5 Conclusion

In this study, we apply a full 4D tomography code for monitoring the variations in the velocities of the rock mass in Kiirunavaara mine, during a period of one month. Our results indicate that monitoring state of stress in the mine through passive seismics can be possible, in principle, given a sufficiently large number of input data (in our case, P- and S- phases arrival times). Adopting a full 4D tomography scheme, i.e. without pre-defined, user-defined time-windows as in time-lapse tomography, we are able to discriminate different phenomena which occur on different time-scales. In particular:

1. We observe relevant V_P velocity increases across the ore-passes, during their activation
2. We do not find an ubiquitous response of the rock mass to blasting activity, in terms of V_P velocity variations
3. We suggest a correlation between V_P velocity recovering and $M_w = 2$ events, related to fluctuation in the local stress-field

Further applications of the full 4D tomography can give more insights into the relation of V_P variations and local stress-changes, analysing data recorded during relevant controlled stress perturbations, e.g. hydro-fracturing operations in mines.

Acknowledgements NPA thanks Daniele Melini for his support in handling parallel jobs on INGV cluster. NPA acknowledges the interesting discussion with Frederik Tillmann on stress changes. Funding for computational resources was provided by LKAB. Partial funding was also provided by SIP-STRIM (Vinnova), Project Number 2016-0269. The computational results presented have been achieved in part using the Vienna Scientific Cluster (VSC-4).

Author contributions N.P.A adapted the algorithm to Kiruna mine data, processed the data and prepared the figures, and wrote the first draft of the manuscript, S.D provided the data and supervised the analysis. C.D provided the mines data and interpreted the elastic models. All authors reviewed the manuscript.

Data Availability No datasets were generated or analysed during the current study.

Declarations

Competing Interests The authors declare no competing interests.

References

Berglund K, Lund B, Tryggvason A, et al (2021) Imaging ore, weak zones and seismically active structures using local event tomography in the Kiirunavaara iron ore mine, Sweden, submitted to XXX

Bhattacharyya A (1943) On a measure of divergence between two statistical populations defined by probability distributions. Bull Calcutta Math Soc 35:99–109

Cai W, Dou L, Gong S (2015) Quantitative analysis of seismic velocity tomography in rock burst hazard assessment. Nat Hazards 75:2453–2465

Caló M, Dorbath C, Cornet F et al (2011) Large-scale aseismic motion identified through 4-D P-wave tomography. Geophysical Journal International 186(3):1295–1314. https://doi.org/10.1111/j.1365-246X.2011.05108.x

Chiarabba C, Gori PD, Boschi E (2009) Pore-pressure migration along a normal-fault system resolved by time-repeated seismic tomography. Geology 37:67–70. https://doi.org/10.1130/G25220A

Dahner C, Dineva S (2020) Small-scale variations in mining-induced stresses, monitored in a seismically active underground mine. In: Wesseloo J (ed) Proceedings of the Second International Conference on Underground Mining Technology. Australian Centre for Geomechanics, pp 233–246. https://doi.org/10.36487/ACG_repo/2035_09, https://papers.acg.uwa.edu.au/p/2035_09_Dahner/

Gallagher K, Charvin K, Nielsen S et al (2009) Markov chain Monte Carlo (MCMC) sampling methods to determine optimal models, model resolution and model choice for Earth science problems. Marine Petrol Geo 26:525–535

Giacomuzzi G, Chiarabba C, Bianco F et al (2024) Tracking transient changes in the plumbing system at campi flegrei caldera. Earth Planet Sci Lett 637(118):74 https://doi.org/10.1016/j.epsl.2024.118744, https://www.sciencedirect.com/science/article/pii/S0012821X24001778

Giacomuzzi G, Chiarabba C, Fronzetti R, et al (2025) Tracking magma migration at campi flegrei caldera, submitted to Science

Kissling E, Ellsworth WL, Eberhart-Phillips D, et al (1994) Initial reference models in local earthquake tomography. J Geophys Res 99(B10):19635–19646

Malinverno A (2002) Parsimonious Bayesian Markov chain Monte Carlo inversion in a nonlinear geophysical problem. Geophys J Int 151(3):675–688

Ma X, Westman E, Counter D (2020) Passive seismic imaging of stress evolution with mining-induced seismicity at hard-rock deep mines. Rock Mech Rock Eng 53:2789â¡80¿¡93¿2804. https://doi.org/10.1007/s00603-020-02076-5

Piana Agostinetti N (2021) Workflow for a full 4d travel-time tomography. RG, https://doi.org/10.13140/RG.2.2.12781.31201/1

Piana Agostinetti N, Calo M (2014) Close-up to the stimulation phase of a egs geothermal site: mapping the time-evolution of the subsurface elastic parameters using a trans-dimensional monte carlo approach. In: EGU General Assembly 2014, EGU, eGU2014-10769

Piana Agostinetti N, Calo M (2015) Refined event location and lowered uncertainties in temporal variation of seismic velocity: tackling down the spatial and temporal correlation between elastic and hypocentral parameters in full 4D local earthquake tomography of a geothermal site. In: EGU General Assembly 2015, EGU, eGU2015-8454

Piana Agostinetti N, Giacomuzzi G, Malinverno A (2015) Local 3D earthquake tomography by trans-dimensional Monte Carlo sampling. Geophys J Int 201:1598–1617. https://doi.org/10.1093/gji/ggv084

Piana Agostinetti N, Malinverno A, Bodin T, et al (2023) Weighing geophysical data with trans-dimensional algorithms: An earthquake location case study. Geophys Res Lett 50(22):e2023GL102983. https://doi.org/10.1029/2023GL102983

Qian J, Zhang H, Westman E (2018) New time-lapse seismic tomographic scheme based on double-difference tomography and its application in monitoring temporal velocity variations caused by underground coal mining. Geophys J Int 215(3):2093–2104. https://doi.org/10.1093/gji/ggy404

Ray S (1989) On a theoretical property of the bhattacharyya coefficient as a feature evaluation criterion. Pattern Recogn Lett 9:315–319

Riva F, Piana Agostinetti N, Marzorati S, et al (2024) The microseismicity of co. donegal (ireland): Defining baseline seismicity in a region of slow lithospheric deformation. Terra Nova 36(1):62–76. https://doi.org/10.1111/ter.12691

Sambridge M, Gallagher K, Jackson A, et al (2006) Trans-dimensional inverse problems, model comparison and the evidence. Geophys J Int 167(2):528–542. https://doi.org/10.1111/j.1365-246X.2006.03155.x.

Young RP, Maxwell SC (1992) Seismic characterization of a highly stressed rock mass using tomographic imaging and induced seismicity. J Geophys Res: Solid Earth 97(B9):12361–12373. https://doi.org/10.1029/92JB00678